U.S. Department
of Transportation
Federal Railroad
Administration

Office of Research,
Development and Technology
Washington, DC 20590

Ballast Fouling Measurement Tool – Phase II

DOT/FRA/ORD-24/22

Final Report | May 2024

REPORT DOCUMENTATION PAGE

Form Approved
OMB No. 0704-0188

1. AGENCY USE ONLY (Leave blank)	2. REPORT DATE	3. REPORT TYPE AND DATES COVERED
	February 2020	Technical Report, July 2016-Dec 2017

4. TITLE AND SUBTITLE
Ballast Fouling Measurement Tool – Phase II

5. FUNDING NUMBERS

6. AUTHOR(S)
Charles P. Oden, Carlton L. Ho, Aaron J. Rubin

7. PERFORMING ORGANIZATION NAME(S) AND ADDRESS(ES)
Earth Science Systems, LLC
11485 W I-70 Frontage Rd., Unit B
Wheat Ridge, CO 80033

8. PERFORMING ORGANIZATION REPORT NUMBER

9. SPONSORING/MONITORING AGENCY NAME(S) AND ADDRESS(ES)
U.S. Department of Transportation
Federal Railroad Administration
Office of Railroad Policy and Development
Office of Research, Development and Technology
Washington, DC 20590

10. SPONSORING/MONITORING AGENCY REPORT NUMBER
DOT/FRA/ORD-24/22

11. SUPPLEMENTARY NOTES
COR: Jay Baillargeon

12a. DISTRIBUTION/AVAILABILITY STATEMENT
This document is available to the public through the FRA eLibrary.

12b. DISTRIBUTION CODE

13. ABSTRACT (Maximum 200 words)
Researchers developed a second-generation RAdar Ballast Inspection Tool (RABIT) using ground-penetrating radar (GPR) for use by track inspectors. This system is much lighter (26 lbs/11.8 kg) than its predecessor (63 lb/29 kg) and is truly portable. It has a single bi-static antenna pair that straddles the tie so the ballast properties under the tie can be measured. During a measurement, the RABIT rolls down the track and obtains average ballast properties over a span of 10 cribs, thereby reducing problems associated with local variability in ballast properties and tie geometry. Researchers constructed a test track with known ballast properties and known fouling and moisture properties ranging from 0-30 percent and 0-4.5 percent by weight, respectively. A neural network was trained to map GPR waveforms to ballast fouling and moisture. The correlation factor between the RABIT estimates and measured values determined from physical ballast samples was better than 0.9. Researchers are planning further testing on in-service track to further validate the approach.

14. SUBJECT TERMS	15. NUMBER OF PAGES
Ground-penetrating radar, ballast, fouling, moisture	30
	16. PRICE CODE

17. SECURITY CLASSIFICATION OF REPORT	18. SECURITY CLASSIFICATION OF THIS PAGE	19. SECURITY CLASSIFICATION OF ABSTRACT	20. LIMITATION OF ABSTRACT
Unclassified	Unclassified	Unclassified	

NSN 7540-01-280-5500

Standard Form 298 (Rev. 2-89)
Prescribed by ANSI Std. 239-18
298-102

METRIC/ENGLISH CONVERSION FACTORS

ENGLISH TO METRIC

LENGTH (APPROXIMATE)

1 inch (in)	=	2.5 centimeters (cm)
1 foot (ft)	=	30 centimeters (cm)
1 yard (yd)	=	0.9 meter (m)
1 mile (mi)	=	1.6 kilometers (km)

AREA (APPROXIMATE)

1 square inch (sq in, in^2)	=	6.5 square centimeters (cm^2)
1 square foot (sqft, ft^2)	=	0.09 square meter (m^2)
1 square yard (sqyd, yd^2)	=	0.8 square meter (m^2)
1 square mile (sq mi, mi^2)	=	2.6 square kilometers (km^2)
1 acre = 0.4 hectare (he)	=	4,000 square meters (m^2)

MASS - WEIGHT (APPROXIMATE)

1 ounce (oz)	=	28 grams (gm)
1 pound (lb)	=	0.45 kilogram (kg)
1 short ton = 2,000 pounds (lb)	=	0.9 tonne (t)

VOLUME (APPROXIMATE)

1 teaspoon (tsp)	=	5 milliliters (ml)
1 tablespoon (tbsp)	=	15 milliliters (ml)
1 fluid ounce (floz)	=	30 milliliters (ml)
1 cup (c)	=	0.24 liter (l)
1 pint (pt)	=	0.47 liter (l)
1 quart (qt)	=	0.96 liter (l)
1 gallon (gal)	=	3.8 liters (l)
1 cubic foot (cu ft, ft^3)	=	0.03 cubic meter (m^3)
1 cubic yard (cu yd, yd^3)	=	0.76 cubic meter (m^3)

TEMPERATURE (EXACT)

[(x-32)(5/9)] °F = y °C

METRIC TO ENGLISH

LENGTH (APPROXIMATE)

1 millimeter (mm)	=	0.04 inch (in)
1 centimeter (cm)	=	0.4 inch (in)
1 meter (m)	=	3.3 feet (ft)
1 meter (m)	=	1.1 yards (yd)
1 kilometer (km)	=	0.6 mile (mi)

AREA (APPROXIMATE)

1 square centimeter (cm^2)	=	0.16 square inch (sq in, in^2)
1 square meter (m^2)	=	1.2 square yards (sqyd, yd^2)
1 square kilometer (km^2)	=	0.4 square mile (sq mi, mi^2)
10,000 square meters (m^2)	=	1 hectare (ha) = 2.5 acres

MASS - WEIGHT (APPROXIMATE)

1 gram (gm)	=	0.036 ounce (oz)
1 kilogram (kg)	=	2.2 pounds (lb)
1 tonne (t)	=	1,000 kilograms (kg)
	=	1.1 short tons

VOLUME (APPROXIMATE)

1 milliliter (ml)	=	0.03 fluid ounce (floz)
1 liter (l)	=	2.1 pints (pt)
1 liter (l)	=	1.06 quarts (qt)
1 liter (l)	=	0.26 gallon (gal)
1 cubic meter (m^3)	=	36 cubic feet (cu ft, ft^3)
1 cubic meter (m^3)	=	1.3 cubic yards (cu yd, yd^3)

TEMPERATURE (EXACT)

[(9/5) y + 32] °C = x °F

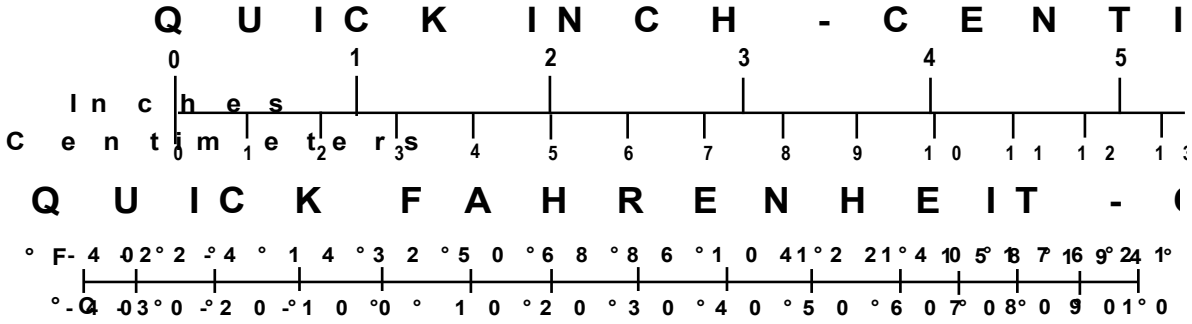

For more exact and or other conversion factors, see NIST Miscellaneous Publication 286, Units of Weights and Measures. Price $2.50 SD Catalog No. C13 10286

Updated 6/17/98

Acknowledgements

The authors acknowledge Hugh Thompson and Gary Carr (retired) of the U.S. Department of Transportation's Federal Railroad Administration and Ted Sussmann of the U.S. Department of Transportation's Volpe National Transportation System Center for their support, advice and assistance during this activity. The authors also acknowledge BNSF Railway for providing access to track for measuring and collecting ballast samples.

Contents

Illustrations

Tables

Executive Summary

Earth Science Systems, LLC (ESS) built a second-generation, portable ground-penetrating radar (GPR) system called the RAdar Ballast Inspection Tool (RABIT) so track inspectors could non-destructively assess ballast fouling and moisture conditions. In August and September 2017, researchers successfully demonstrated the prototype system using a test track constructed by BNSF Railway at their research facility in Topeka, KS. The fouling and moisture content of the test track ballast ranged between 0-30 percent and 0-4.5 percent by weight, respectively. The team trained a neural network to map GPR waveforms to ballast fouling and moisture estimates. The correlation coefficient between the RABIT estimates and measured values determined from physical ballast samples was greater than 0.9. Although initial tests succeeded, further testing is necessary to ensure that the neural network estimator has not been trained on site-specific features, and that it can be used throughout the in-service rail network. During the next project phase, the research team will conduct further testing on in-service track and implement improved algorithms. The goal of the upcoming phase is to assess system performance in a variety of common track conditions. This report covers the second year of a three-year project.

The previous RABIT prototype weighed 63 lb (29 kg), which was heavier and larger than desired. This system contained a transmitting antenna and two receiving antennas operating at 450 MHz and a second set of antennas with the same arrangement operating at 2 GHz. With this system, antennas placed directly on the ballast surface made "spot" measurements. Previous tests showed 1) significant variability on the GPR response from "spot" to "spot," 2) most of the information contained in the 2 GHz data could be obtained from the 450 MHz data, and 3) the 450 MHz data provided valuable depth and thickness information that could not be obtained from the 2 GHz data. Therefore, ESS built the second-generation RABIT with only 500 MHz antennas, where the transmitting antenna and first receiving antenna are located on the gage side of the rail, and the second receiving antenna is on the field side of the rail. This unit incorporates a cart that is rolled down the track, obtaining an average measurement over a number of cribs (e.g., 10 cribs), thereby reducing problems associated with local variability in ballast properties and tie geometry. To allow free movement along the track, the bottoms of the antennas were placed 2 inches above the surface. Tests with the second-generation RABIT showed data from the receiving antenna located on the field side of the rail had a much poorer signal quality than data from the inside receiver antenna. Therefore, ESS removed the field side antenna. Currently, the RABIT has only one transmitting antenna and one receiving antenna, reducing the unit weight (26 lb/11.8 kg) and increasing portability.

The results from the second year are encouraging and show that moisture and fouling can be successfully measured with non-invasive methods. Although the RABIT instrument and analysis routines performed well in tests to date, the system needs continued verification, testing, and adjustments to demonstrate that it can be applied in most field conditions. For more background on this project, see Phase I of this project (FRA, 2014).

1. Introduction

1.1 Background

Ballast fouling is one of the primary causes of subsurface support structure degradation in railways. It lowers resistance to forces applied by the ties and reduces resilient modulus and energy absorption capacity (Selig and Waters, 1994). Previous research (Silvast et al., 2010; Al-Qadi et al., 2007) has shown that ground-penetrating radar (GPR) is a promising technique for investigating the condition of railway ballast and subgrades. The purpose of this project is to expand on this previous research and provide a more quantitative assessment of ballast condition.

This project seeks to develop a non-invasive ballast inspection method that can be used by railroad track inspectors. Earth Science Systems, LLC (ESS) developed an instrument that can make the required measurements without disturbing or removing any ballast. In accordance with FRA recommendations, the developed instrument is lightweight (26 lb/11.8 kg) and can be carried by one person. The instrument estimates the weight fraction of fouling material and moisture present in the ballast. Additionally, researchers examined methods for estimating other useful properties of the ballast, such as the Selig fouling index (Selig and Waters, 1994) and ballast depth.

1.2 Objectives

The objectives of this phase of the project are listed below:

- Design a truly portable second-generation RABIT.
- Show that a single set of 500 MHz antennas is sufficient for providing robust estimates of ballast fouling and moisture.
- Demonstrate that by taking continuous measurements over several cribs (e.g., 10 cribs), local variations (i.e., within a single crib) in ballast properties and tie geometry do not significantly skew the readings.
- Demonstrate a strong correlation between ballast properties determined from physical samples and estimates provided by the RABIT.
- Plan a field testing program that will demonstrate the value of the new tool, and encourage adoption by industry.
- Investigate the relationships of the properties measured by the RABIT to other ballast properties, such as elastic modulus and yield strength.

1.3 Scope

This project examines the viability of using ground-coupled GPR for ballast inspection. The research team intentionally did not consider air-coupled and mobile radar units that are operated from hi-rail vehicles, geometry cars, and other rolling stock; but rather focused on creating a smaller man-portable unit. The use of air-coupled GPR has been studied extensively (Silvast et al., 2010; Al-Qadi et al., 2007). Although a more complete picture of the ballast and sub-ballast could be obtained with an array of antennas spanning from one shoulder to the other, and possibly spanning multiple cribs, such a system would not be portable. Because the RABIT is designed to take localized measurements of fouling and moisture, we will not attempt to identify continuous subsurface structures that require measurements over length scales greater than a few meters, such as continuous layer boundaries, ballast pockets, and clay lenses.

1.4 Overall Approach

The researchers' first task was the design and construction of a second-generation RABIT instrument with a reduction in weight and increase in portability. To assist in this task, the researcher's added the ability to roll down the track and obtain an average reading over several cribs to the design. The system makes use of newly developed antenna technology by ESS that enables construction of smaller and more lightweight antennas.

The second task was to build a test track with a range of different ballast properties and conduct field tests with the RABIT. BNSF built such a test track at its research facility in Topeka, KS. Researchers took a series of measurements with the RABIT, which were then followed by in-place geotechnical tests and finally physical sample extraction. The actual ballast properties were determined from laboratory measurements.

The third task was to develop analysis algorithms tailored to the second-generation RABIT. These routines were designed to both average the readings over the span of a few cribs and be tolerant to variable tie placement. An approach based on neural networks worked well in initial testing.

The team's final task was to make hardware adjustments to the RABIT to increase its portability and prepare it for field testing on revenue service track (which will occur in the third phase of this project).

1.5 Organization of the Report

This report covers the design and construction of the basic technologies involved in the RABIT system. Section 2 discusses the background and hardware design of the portable GPR unit. Section 3 presents construction and testing of a test track and summarizes of field testing efforts. Section 4 discusses data analysis and system assessment. Section 5 summarizes the findings, presents conclusions, and offers suggestions for further research. This report presents each section in chronological order to the work being performed.

2. GPR Background and RABIT Hardware Design

The following sub-sections present the scientific background for the application of GPR technology for railroad ballast inspection as well as a detailed overview and associated technical discussion of the development and construction of the working prototype of the portable GPR unit used in this study.

2.1 GPR Response to Ballast Material

GPRs transmit temporally compact electromagnetic (EM) wavelets that travel through the media in a direct or reflected wave path and arrive at the receiver after some delay and with some attenuation. When a radar's transmitting and receiving antenna are placed on or near the ground with a constant offset between them (i.e., a bi-static antenna configuration), a direct wave travels between the antennas through the air, another direct wave travels through the ground, and reflected waves occur when incident waves bounce off subsurface (or above the surface) media with differing EM properties. With knowledge of the wave path and the measured travel time and attenuation, the EM properties of the media along the wave path can be deduced (see Figure 1).

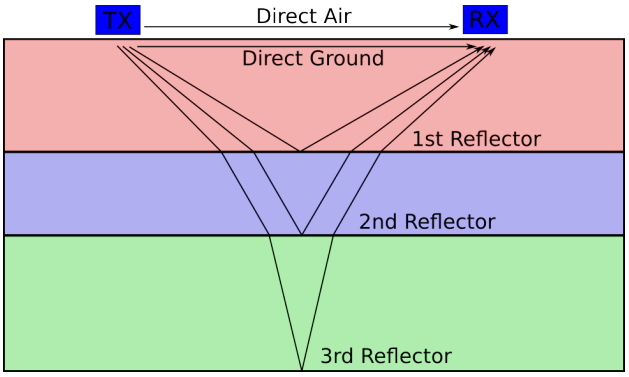

Figure 1. Ray paths for waves for a GPR survey in layered media.

The attenuation of EM waves occurs when a medium absorbs energy (as in a microwave oven), and when the waves scatter out of the travel path being considered. This scattering can be specular or diffuse. Specular scattering occurs when waves bounce off surfaces that are much larger than a wavelength (e.g., the bottom of a horizontal subsurface layer), and diffuse volume scattering occurs when the surfaces are smaller, or similar to, a wavelength in size (e.g., voids between the aggregate). All waves experience wavefront spreading where the amplitude decays as r^{-2} from the transmitting antenna (r is distance from the antenna).

The travel time of an EM wave depends on the wave velocity of the medium, which in turn depends on the dielectric constant (which can be frequency-dependent). The dielectric constant of ballast material depends on the type of aggregate material, the amount of fines filling the voids, and the moisture content. In a layered medium, the travel time of a reflected wave recorded using a pair of antennas (one for transmitting and the other for receiving) at a fixed offset does not provide enough information to determine both layer thickness and wave velocity. However, if the dielectric constant can be estimated by other means (i.e., wave shape, attenuation versus frequency, etc.), then it is possible to estimate layer thicknesses.

The shape of the early waveforms that arrive before the reflected waves is a combination of the direct air waves and ground waves. These waveforms are complex and difficult to model from a physics-based approach (Oden, 2006); however, they do contain useful information and can be interpreted in a heuristic manner.

GPR surveys can be conducted over a wide range of frequencies (and wavelengths), but generally are performed in the 50 MHz to 2 GHz range. The EM wavelength in ballast materials is mostly a function of moisture content but is also sensitive to fouling. For dry earth, the wavelengths at 50 MHz and 2 GHz are typically 118.1 inches and 3.0 inches (300 cm and 7.5 cm), respectively, and 47.2 inches and 1.2 inches (120 cm and 3 cm) for wet earth. At low frequencies, the penetration is good when conductivity is low but the resolution is poor. At high frequencies, the resolution is good, but diffuse volume scattering can cause significant attenuation. Volume scattering occurs when the particle (aggregate or voids) is similar in size to a wavelength. In general, there is a frequency window within which GPR works well. At low frequencies, the attenuation (per wavelength) increases with increasing conductivity and decreasing frequency. At high frequencies, attenuation increases with increasing aggregate or void size and with increasing electrical contrast between the aggregate and voids. Additionally, as frequency increases above 1 GHz, the attenuation due to the dielectric relaxation of water increases. As a result, GPR surveys are commonly operated in the 50 MHz to 2 GHz range.

GPR surveys can be conducted using ground-coupled or air-coupled antennas. When the antenna is within a quarter wavelength from the ground (59 inches/150 cm at 50 MHz and 1.48 inches/3.75 cm at 2 GHz) the antennas are considered ground-coupled. When the antennas are greater than a wavelength from the ground (236.2 inches/6 m at 50 MHz and 5.9 inches/15 cm at 2 GHz) they are considered air-coupled. When using ground-coupled antennas, the shallow ground under the antennas becomes part of the antenna, and therefore the antenna response changes as the shallow ground properties change. Surface roughness and variable shallow ground properties affect the quality and repeatability of ground-coupled GPR measurements. Ground-coupled antennas can transmit more energy into the subsurface than air-launched antennas, and subsequently they provide a greater penetration depth. Air-launched antennas have the benefit of constant response and are better-suited for use from a mobile platform such as a hi-rail vehicle.

In ballast materials, it is known that both moisture and fouling affect the propagation velocity and attenuation of EM waves. Consider Figure 2, where the 450 MHz EM wave velocity (normalized to the velocity in free space) and the 2 GHz scattered amplitude (relative to a solid non-porous medium) are plotted versus the volume fraction of fouling material and moisture. From the field capacity studies described in FRA (2014), it is known that one part moisture requires approximately two parts fouling material to hold it in place, therefore the lower-right corners of the plots are blank because this scenario cannot occur (i.e., cannot have more moisture than the ballast can hold). The plotted ranges of fouling material and moisture span the values that commonly occur in ballast. The velocity plot was calculated using EM mixing laws (FRA, 2014). For the high-frequency scattered amplitude there are two phenomena that affect the GPR scans: volume scattering due to contrasting EM properties between the aggregate and the voids and dielectric absorption by water. These phenomena are difficult to accurately model, so the plot shows a heuristic representation of these effects based on contrast and moisture content. Note that both EM velocity and scattered amplitude have some sensitivity to fouling material, but are most sensitive to changing moisture content. A simple velocity or scattered amplitude

measurement alone does not provide enough information to assess both fouling and moisture content. Furthermore, since the contours on both plots are similar, the combination of both measurements does not provide enough information to provide reliable estimates of both fouling and moisture. In essence, a purely physics-based approach using reflected wave velocity and attenuation mainly provides a good indication of moisture content and fouling to a lesser extent. From this analysis, researchers concluded that the algorithm providing robust estimates of both fouling and moisture would be based on a heuristic approach that includes the entire waveform (e.g., direct air waves, direct ground waves, and reflected waves).

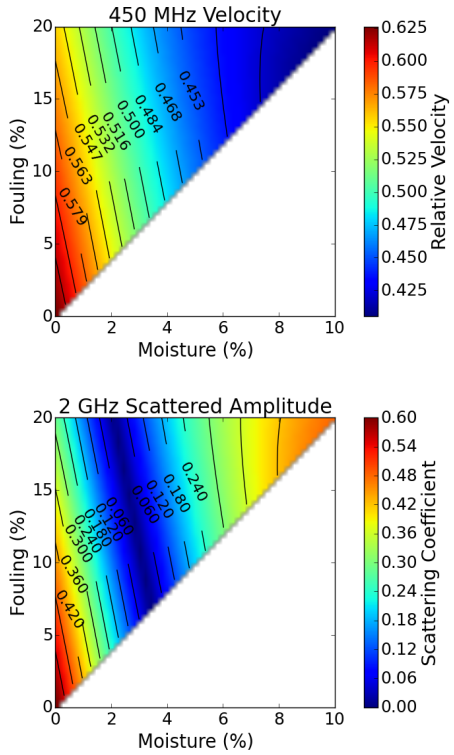

Figure 2. EM wave velocity and backscatter amplitude vs. fouling and moisture as predicted by equivalent media-mixing law relationships.

2.2 RABIT Design and Prototype

After considering the phenomena above, researchers concluded that the second-generation RABIT should certainly employ 500 MHz antennas, and that since the 2 GHz antennas do not provide much additional information, they can be eliminated to save weight. The 500 MHz antennas provide a signal that penetrates sufficiently to obtain reflections from the bottom of the ballast layer, and at times from the bottom of the sub-ballast as well. The newly developed ESS 500 MHz antenna technology provides a broadband response that extends to frequencies as high as 900 MHz, where attenuation by volume scattering of ballast voids can be observed. Figure 3 shows the second generation RABIT configuration. One bi-static antenna pair (one transmitting and one receiving antenna) was set up to measure the ballast under the tie, and the other bi-static pair was set up to measure under the rail, because the ballast conditions can be different in these two regions. The yellow frame was constructed from lightweight fiberglass tubing to reduce weight.

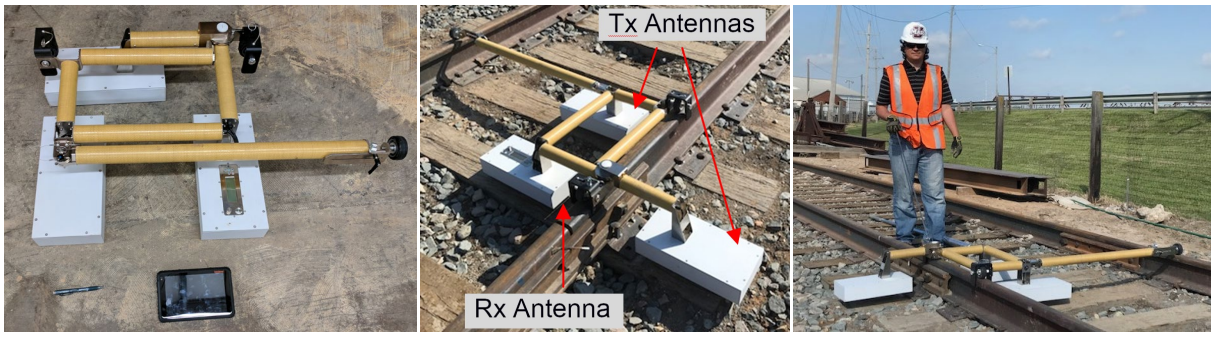

Figure 3. Left panel shows the RABIT folded and ready for transport, and the center and right panels show the RABIT setup for surveying. The antennas are located inside the white boxes.

The second-generation design included many features to make it easy to use in the field. Wheels on the measurement frame allow the user to easily push or pull it along the track while an adjustable outrigger allows it to accommodate different track gages. It was designed for a rail height of 7.625 inches (19.4 cm) with a 0.875-inch (2.2 cm) thick tie plate, a tie spacing of 19 inches (48.3 cm). It contains an internal battery that provides power for 3 to 4 hours of continuous operation.

Experiments conducted with the initial RABIT prototype during the first year of this project indicated that the rails do not cause significant interference to the signals from the antennas as long as the antennas were on the same side of the rail and at least 4 inches away from the rail. Since the current focus is on tracks with timber ties, the antenna configuration and analysis routines were tailored accordingly. For tracks with concrete ties that contain rebar or use non-standard tie spacing, there may be unwanted signal interference that could require further experiments and development of specific analysis algorithms.

Tests to evaluate the RABIT response were conducted on a test track (see Section 3). Measurements made with the receiver antenna located on the field side and the transmitting antenna on the gage side of the rail had small amplitudes and significant noise, probably due to signal attenuation by the rail. Because of the reduced quality of this data and the desire for a light-weight instrument, researchers decided that the field-side antenna could be removed. The result is the configuration shown in Figure 4. The current weight of the unit is 26 lb (11.8 kg), and the folded dimensions are 27 by 30 by 11 inches (68.6 by 76.2 by 27.9 cm).

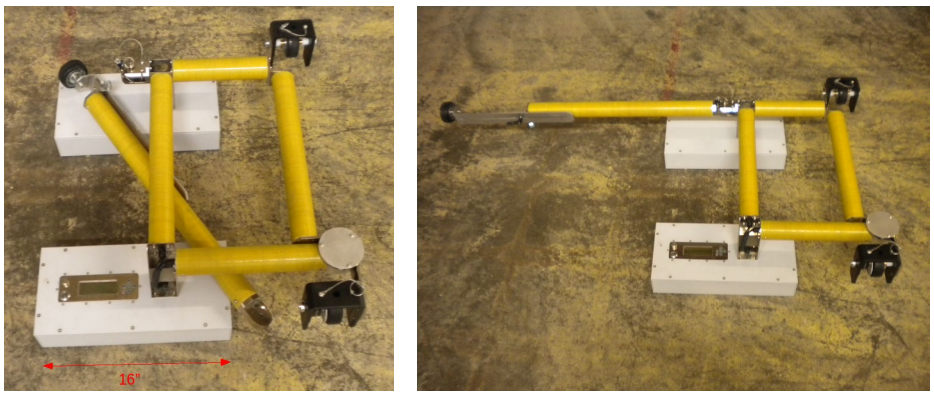

Figure 4. Final RABIT configuration folded for transport (left), and with extended outrigger (right). The antennas are positioned 6 inches (15 cm) from the side of the rails.

3. Test Track

This section presents an overview of the field testing conducted as part of this study. The first sub-section gives a detailed description of the construction of the test track at the BNSF research facility in Topeka, KS, which was instrumental in the preliminary testing of the RABIT prototype. The later sub-sections provide a summary of the results associated with the field testing, including measurements of track stiffness and modulus versus fouling and moisture as well as the data collected by the GPR system.

3.1 Building the Test Track

A test track was built at the BNSF research facility in Topeka, KS with a range of ballast conditions. The test section was 60 feet long, divided into 15-foot sections, each with different fouling levels. Figure 5 contains a photograph and a diagram of the test track. During construction of the test track, four granitic ballast mixtures were made, each with a different fouling level (nominally 0 percent, 10 percent, 20 percent, and 30 percent by weight) using granitic dust as fouling material. Construction started by laying down and compacting ballast to a thickness of 17 – 25 inches (43.2 – 64.5 cm). Then the ties and rail were placed. Finally, the ballast in the cribs was added and compacted with a hand-held tamper rather than by machine. The result was that the ballast below the ties was likely better compacted that the ballast between the ties. Ties were placed at a center-to-center spacing of approximately 18 to 20 inches (45.7 – 50.8 cm) with local variations of +/- 3 inches (7.6 cm) which is not atypical for in-service track.

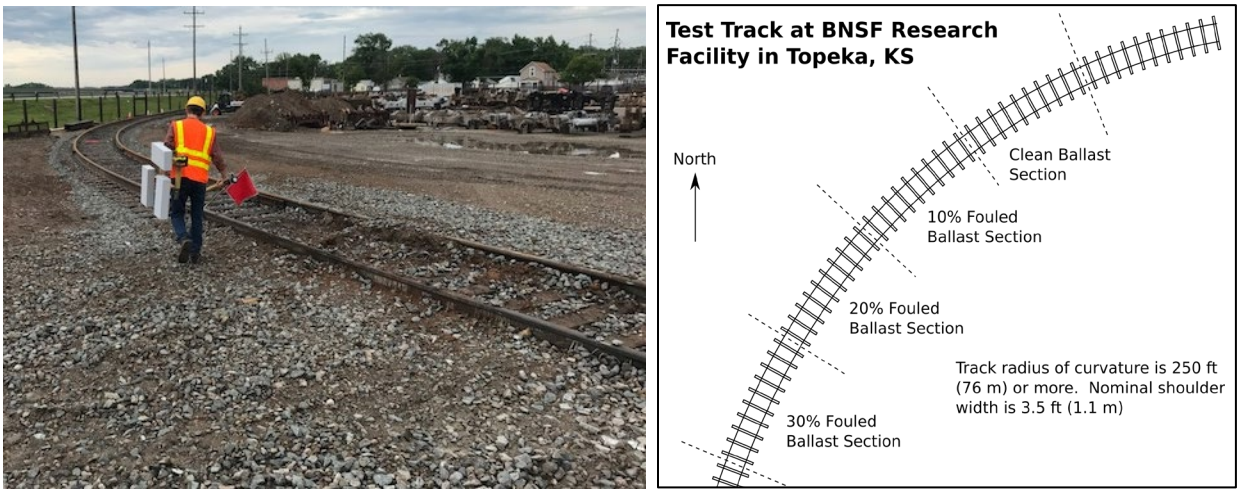

Figure 5. View of the test track to the northeast (left) and layout diagram (right).

The test track was also subjected to different moisture levels — "low moisture," "mid moisture," and "high moisture" — as described below. With each fouling-moisture combination, in-situ measurements were made using the RABIT, a lightweight deflectometer (LDW), and a dynamic cone penetrometer (DCP). Finally, physical samples were taken and subjected to standard laboratory tests to determine density, moisture content, and grain-size distribution. Consult Rubin et al. (2018) for more details.

3.2 Wetting the Test Track

Measurements on the test track were made at the three aforementioned moisture conditions (see Table 1 for actual values). Controlling the moisture of the outdoor track was more difficult than with the indoor track used for the first phase of this project. The indoor, full-scale track model was constructed with varying ballast fouling levels and was then carefully irrigated to arrive at certain moisture levels. With an outdoor test track, natural precipitation events and slow drainage rates made it more difficult to control the moisture level. ESS conducted field measurements over a 4-week period in early summer after numerous recent and heavy rainfall events. The first test at the mid-moisture level was conducted 2 days after a heavy rain. For the low-moisture level, tests were performed after the test track was allowed to drain for 1 week without precipitation. Drying of the ballast occurred at a slow rate because the test track was built on very clay-rich, water-saturated soil near the Kansas River in Topeka that was not conducive to drainage, and because the ambient humidity was high. For the final high-moisture level, the test track was irrigated to field capacity and covered, allowing the moisture distribution to reach equilibrium overnight.

Table 1. Fouling and Moisture Values for the Test Track

Fouling / Moisture	0% Fouling	10% Fouling	20% Fouling	30% Fouling	Notes
Low Moisture	1.22 / 0.29	3.82 / 0.58	23.4 / 1.81	47.5 / 3.35	Allowed track to drain for 1 week following a rain event
Mid Moisture	0.20 / 0.57	3.74 / 1.25	13.3 / 1.96	37.8 / 1.23	Initial field conditions after recent rain event
High Moisture	0.58 / 0.95	10.1 / 2.81	22.1 / 4.18	36.6 / 4.56	Irrigated to field capacity

3.3 LWD and DCP Data Collection

A LWD from Olson Instruments was used to measure stiffness and modulus for each fouling-moisture condition. The LWD employed a 22 lb (10 kg) weight falling from a 23.6 inch (60 cm) drop height, an embedded load cell and geophone, and a 7.87 inch (20 cm) diameter plate (see Figure 6). A tablet computer was used to acquire and process LWD data. The geophone measured the plate deflection, the load cell measured impact force, and the instrument's software calculated stiffness and elastic modulus. Researchers took LWD measurements in-between each tie location along the test track, except when tie spacing was too close to fit the 7.87 inch (20 cm) diameter plate (tie spacing and alignment varied – see Figure 10 for an example). At each location, the LWD applied three seating drops to the plate before applying three measurement drops. ESS calculated stiffness and elastic modulus based on an average of the responses from the three measurement drops.

Figure 6. Lightweight deflectometer (left) and dynamic cone penetrometer (right).

Researchers used a DCP from Kessler Soils Engineering Products, Inc. to measure the California bearing ratio (CBR), which is a penetration test used to evaluate the subgrade strength (Ayers et al., 1989). The DCP incorporated an 8 kg (17.6 lb) hammer, an anvil, a penetration cone with a 60 degree angle and 0.79 inch (2.0 cm) base diameter, and 0.63 inch (1.59 cm) diameter steel rods (Figure 6). The drop height for the hammer was 22.6 inches (57.5 cm). The number of blows required to penetrate consecutive 4-inch (100.0 mm) lengths was recorded for penetration depths of 0 – 40 inches (1 m) below the top of ballast. For each 4-inch (100 mm) segment, the DCP penetration index (*DPI*) was calculated in units of mm/blow, and the *CBR* was then calculated as follows (Webster et al., 1992):

$$CBR = 292/DPI^{1.12}$$

The dynamic elastic modulus in MPa, *E*, was calculated as follows (Powell et al., 1984):

$$E=17.58 \cdot CBR^{0.64}$$

Figure 7 shows plots of the DCP and LWD results for each of the 12 ballast-fouling conditions encountered at the test track (see Table 1). For each condition, a group of circles is plotted at the same point, and both the diameter and color of each circle indicate the value of the measurement. A reduction in stiffness is evident at high moisture values, and the results for mid- or low-moisture values are variable. These preliminary results indicated that the loss of stiffness or modulus did not occur until moisture levels were high; it should be noted that final conclusions cannot be made from such a small amount of data.

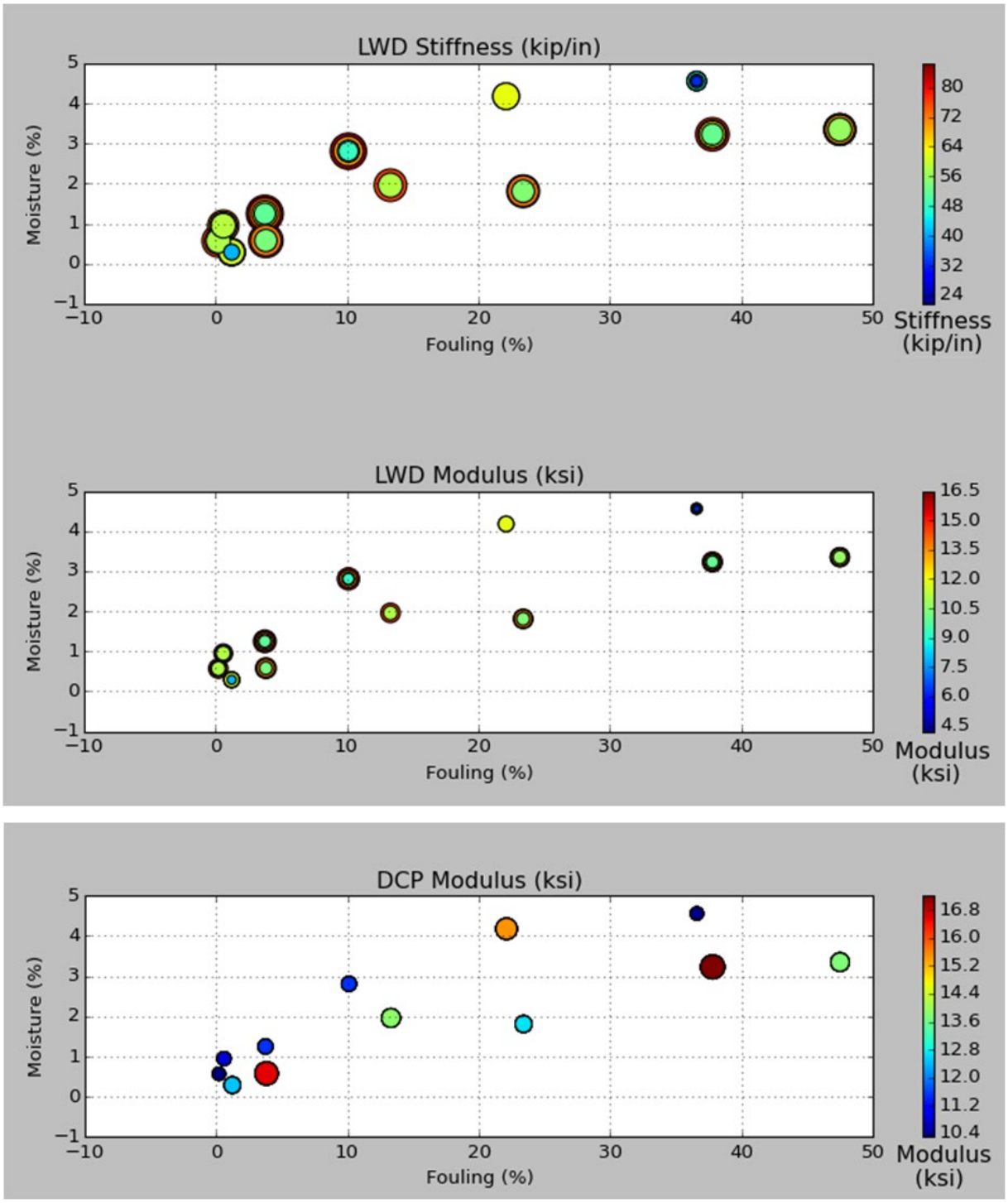

Figure 7. Stiffness and modulus (represented using colors and symbol size) vs. fouling and moisture as measured by the LWD and DCP. Symbol diameter and color both represent modulus, and this combination conveys the variation in measured results for each ballast condition.

3.4 RABIT Data Collection

RABIT collected data for each moisture condition by running the GPR system at walking speed down each side of the entire 60-foot test track using a waveform sampling rate of 50 waveforms per second. Figure 8 below depicts a typical GPR scan image (where each column of pixels represents a single time-series radar waveform). This image was recorded on track with ballast at the mid-moisture condition (see Table 1). The vertical axis is time in nanoseconds and the horizontal axis is an arbitrary time scale. The bright peaks occur when the RABIT antennas evenly straddle a tie and are positioned directly over a crib on each side of the tie. The left side of the image corresponds to a highly fouled condition, and the right side to a clean ballast condition. The variability in the data is evident, but the clean ballast response generally exhibits higher amplitudes and earlier arrival times. There are nine ties in each 15-foot section, but the data from the tie at the boundary between each section was not used because there may be mixing between the different fouled sections. A waveform (i.e., a time series of the received radar wave samples with the antennas at a single location) was manually extracted for each tie location and these waveforms are shown in Figure 9. These are the waveforms that will be used to estimate ballast properties. Researchers assumed that selecting these waveforms would be a simple task that could be done easily by computer, but the variability in the data made manual selection a necessity. To automate this process, a wheel odometer has been added to the RABIT for use in future surveys. The odometer measurements will constrain the selection algorithm so that it does not select waveforms from locations that are atypically close together and lie within the same crib or too far apart and possibly skip a crib.

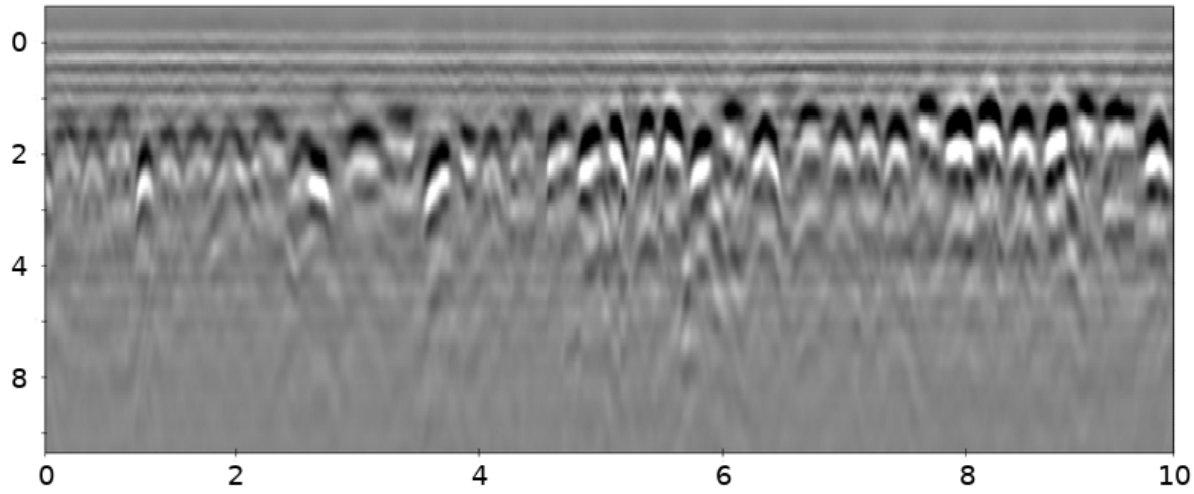

Figure 8. A GPR scan image showing the high amplitude response every time the antennas straddle a tie. The bright peaks occur when the RABIT antennas evenly straddle a tie and are positioned directly over a crib on each side of the tie. The left side of the image corresponds to a highly fouled condition and the right side to a clean ballast condition.

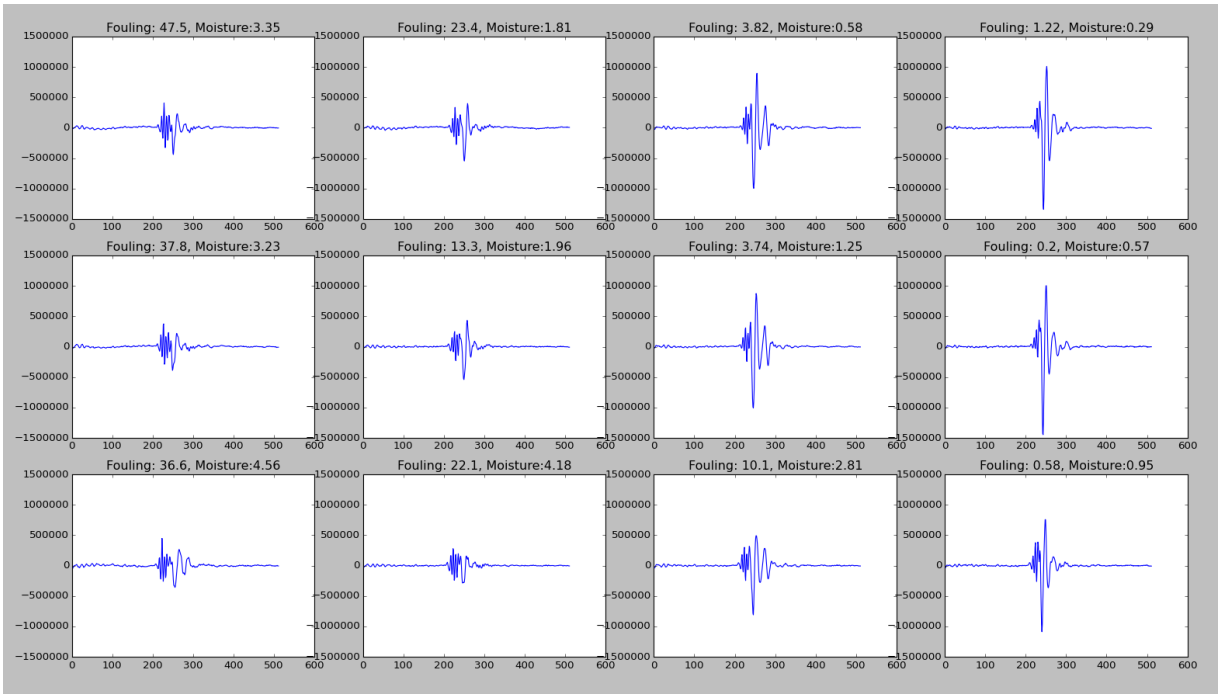

Figure 9. The waveforms extracted for the mid-moisture level test track. The clean ballast response generally exhibits higher amplitudes.

3.5 Measuring the Geotechnical Properties of Ballast

To obtain the ground-truth properties of the ballast material, researchers extracted physical samples for laboratory analysis for each of the 12 fouling-moisture conditions after the DCP, LWD, and RABIT data were collected. For each sample, researchers removed at least 165 lbs (75 kg) of ballast material from one crib. Then to prepare for the next set of tests, the material was replaced using the previously prepared ballast mixtures so that DCP, LWD, and RABIT measurements could be taken at a later time on the same track under different moisture conditions. To preserve as much of the original track structure as possible, no more than one sample was taken from a given crib. Table 1 lists the properties determined by laboratory testing. The column headers indicate the planned fouling level, and the table entries show the actual fouling and moisture levels as determined from standard laboratory tests on the extracted samples. The sampling process followed the method outlined in Yoo et al. (1978). After removing the sample, the sample void was lined with a plastic sheet and filled with water. The volume of water needed to fill the void represented the volume of the sample. The samples were weighed before and after drying to determine moisture content in accordance with ASTM D2216-05 (ASTM, 2007). The dry samples were then sieved to determine the grain-size distribution in accordance with ASTM D6913-04 (ASTM, 2008).

4. RABIT Data Analysis

The following sub-sections describe in detail the analyses, and results of these analyses, performed on the GPR's waveform data collected from the aforementioned test track at the BNSF research facility in Topeka, KS. This method of analysis includes the data preparation, as well as the training and verification of the associated neural network.

4.1 Neural Network Approach

Physical variations in ballast properties and tie geometries, at different locations that are near to each other, may cause "spot" measurements to provide unrepresentative results. The physics-based algorithms created in the first year of this project do not account for ties interfering with the propagating waves and other geometric variations; however, the ray tracing routines and mixing formulas developed in the first phase are useful for estimating auxiliary properties such as ballast thickness and void ratio. Figure 10 shows an example of variability in tie spacing and alignment observed on the test track. The analysis algorithm should be tolerant of this variability, as well as variations in ballast thickness, sub-ballast properties, fouling materials, and tie types (timber versus concrete). Neural networks are known for their ability to recognize complex patterns in data (e.g., speech recognition) and are a good choice for creating ballast property estimators that are tolerant to these environmental variations. Neural network estimators must be trained using training data and then validated using independent test data. In this work, the RABIT data collected on the right side of the track was used to train the network and the data from the left side was used for validation.

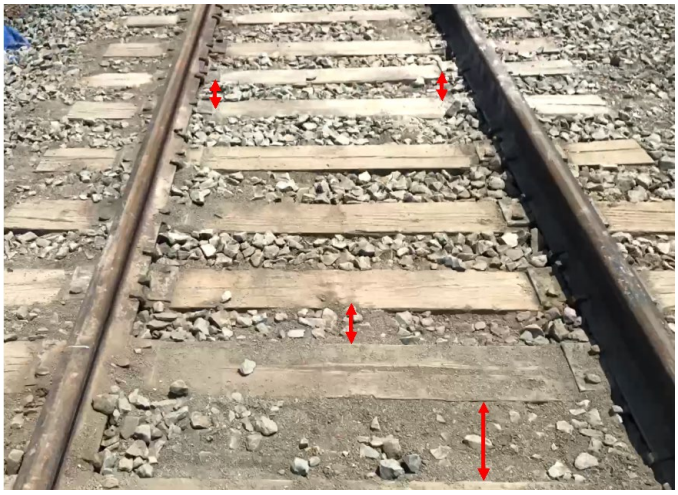

Figure 10. Variable tie spacing and alignment observed on the test track.

Before passing the waveform data to the neural network for training, it needed to be cleaned and pre-processed. The cleaning step ensured that only data with a high signal-to-noise level were used in the training process. This was accomplished by selecting the waveform with the highest amplitude from all the GPR scans over a single tie (see Figure 9). Next, the spectrogram for each waveform is calculated to provide a representative image for each tie (see Figure 11). Each spectrogram has 650 pixels. The training data consisted of 96 spectrograms from 12 different ballast conditions and 8 cribs per ballast condition. The spectrograms show a general trend of

more low-frequency energy partitioning for more fouled conditions (i.e., upper-left plot in Figure 11) and later arrival times for more moist conditions (i.e., lower-left plot in Figure 11).

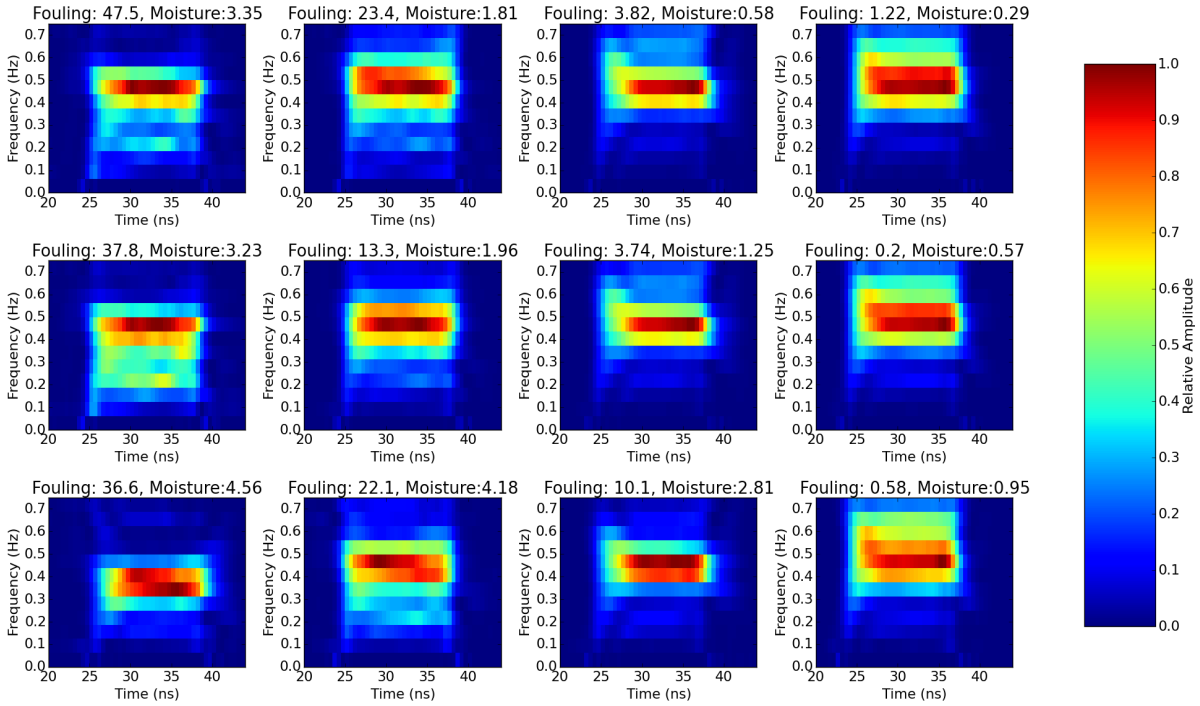

Figure 11. Spectrograms generated from selected waveforms were used as inputs to the neural network.

4.2 Training and Verification

The multi-layer perceptron (MLP, Géron, 2017) network topology (see Figure 12) works well for stationary image classifiers that must recognize complex patterns in the data. A three-layer MLP was selected for this problem with 650 inputs (one for each pixel in the spectrograms), 128 hidden-layer perceptrons, and two output stages – one for moisture estimation and the other for fouling.

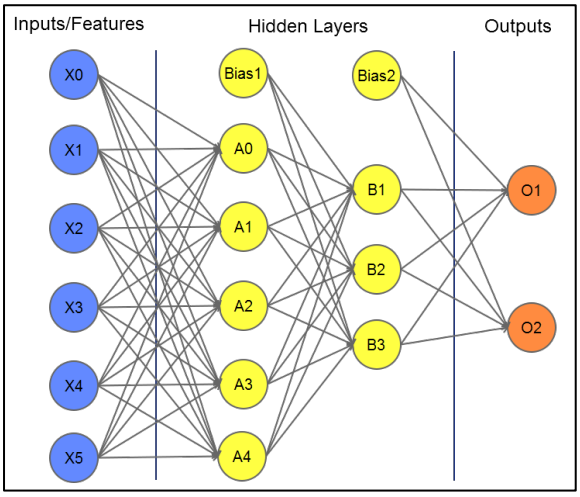

Figure 12. A four-layer MLP.

The output of each perceptron used a rectifier function where positive values are unchanged and negative values are zero. The training phase used the 96 spectrograms from the right side of the track and the network was trained for 1,000 epochs. After training, the weighting coefficients were determined for each perceptron and the network could then be used as an estimator. Consult Géron (2017) and Hagen et al. (2014) for more details on the architecture and training of neural networks.

After training the MLP network, the data from the left side of the track were used for validation. The results are shown in Figure 13. In the upper panel, the predicted moisture and fouling for each tie are plotted against the measured values determined from laboratory testing of extracted samples. When the RABIT data from a single tie is used to estimate moisture and fouling, the results have substantial variability with correlation coefficients of 0.77 and 0.84 respectively. But when the estimated values for 8 ties with the same moisture-fouling condition (see Table 1) are averaged, the correlation coefficients improve to 0.91 and 0.92 for moisture and fouling, respectively. The researchers presumed that the averaging operation reduced sensitivity to local variations in ballast properties (i.e., variations within a single crib), tie geometry, etc. Although these results were encouraging, the MLP could have been recognizing something in the data that reflected an environmental condition other than fouling or moisture. More testing is needed to vet these early results.

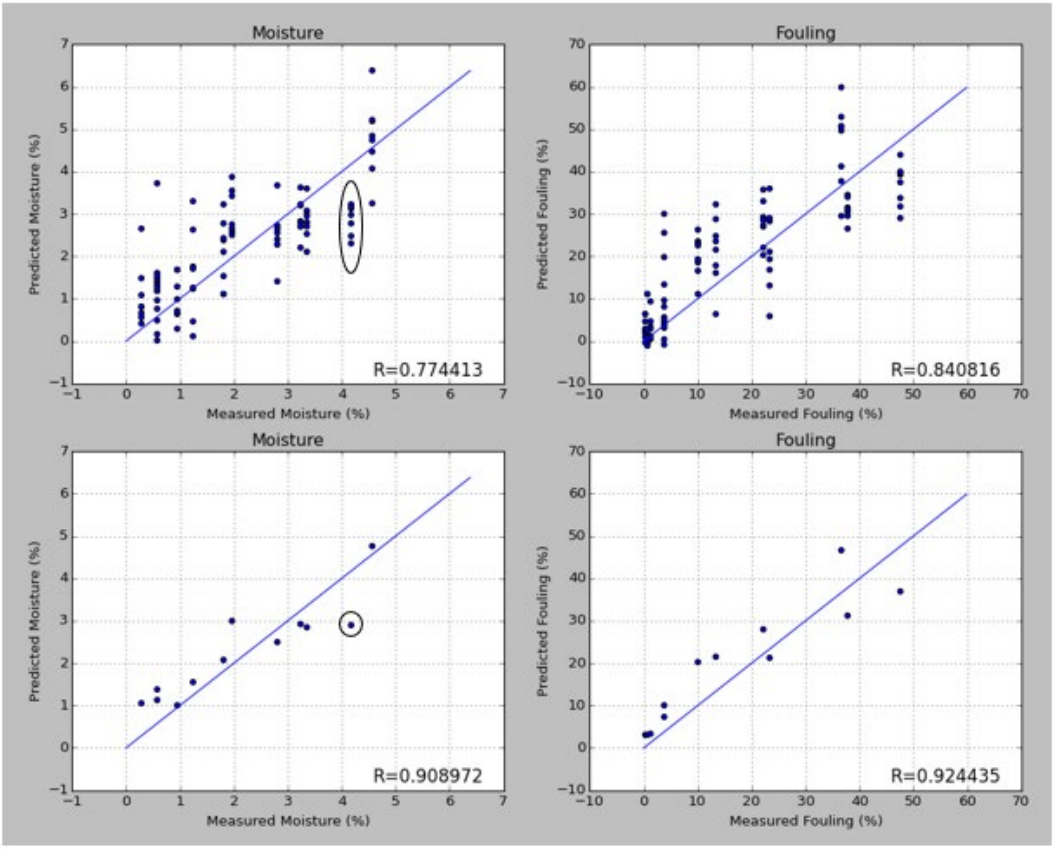

Figure 13. Predicted moisture and fouling versus measured moisture and fouling of physical samples. In the upper plots, each dot is an estimate determined with RABIT waveforms from individual cribs. In the lower plots, each dot is an average of estimates from 8 cribs and corresponds to one of the moisture-fouling conditions listed in Table 1.

5. Conclusion

ESS designed, built, tested, and evaluated data from a second-generation GPR ballast inspection system. The second-generation RABIT system provides a non-invasive method to estimate the amount of fouling and moisture present in in-service track. Early results showed fouling and moisture estimates correlated well with actual values (correlation values of 0.91 and 0.92 for moisture and fouling, respectively) when results were averaged over multiple (8) cribs. Further field testing needs to be performed to evaluate the effectiveness of the equipment and analysis methods proposed under this study.

There are several observations from the current RABIT system:

1. Results indicated that the ability to roll down the track and take continuous readings reduces sensitivity to local variations in tie and ballast geometry and improves the accuracy of moisture and fouling estimates over those obtained from measurements a single fixed location (such as the measurements made in Phase I of this project).
2. The neural network estimator provided moisture and fouling estimates in real time in the field at the time RABIT data were collected.
3. The neural network results to date using RABIT measurements on the gage side of the rail were encouraging, indicating that measurements from a single pair of antennas were sufficient. The RABIT measurements with one antenna on the field side of the rail were of poor quality. Rather than trying to improve the field-side response, ESS removed the field-side antenna to achieve the goal of a lightweight instrument that can be easily carried by one person (26 lb/11.8 kg). However, with this weight reduction, the ability to measure ballast properties on the shoulder is lost.
4. The neural network approach requires a significant amount of training data, but it is tolerant to noisy and variable data, geometry variations, and heterogeneous ballast properties (unlike physics-based approaches). Although the tests thus far indicated tolerance to variable field conditions (such as changing tie spacing), the variability encountered to date did not represent the much larger range of environmental variations expected throughout the country. To achieve robust estimators that work well in a wide variety of conditions, more testing and training under a wide variety of conditions is recommended.
5. At the time the test track data were taken, the RABIT did not have a wheel odometer. This made it necessary to manually pick waveforms from the data for interpretation by the neural network estimator. ESS added an odometer to RABIT to aid in an automatic waveform picking algorithm. The odometer measurements will constrain the picking algorithm so that it does not pick waveforms that are atypically close together or far apart. The utility of such a picking algorithm will be examined as data from future field tests become available.
6. The railroad industry commonly uses the Selig fouling index (SFI) as a measure of fouling. The SFI weights fine-grained material twice and is therefore not a linear volumetric measure of fouling. The physics-based mixing formulas that relate void space and fouling to dielectric and attenuation constants specify in terms of volume fraction. A

neural network does not have these constraints, so in future neural network estimators will be trained to provide SFI.

7. It is likely that neural network estimators can be trained for use with concrete ties if the steel strands do not significantly degrade the radar signal.
8. The electromagnetic properties of fouling material derived from granite, limestone, and coal are very similar, and it is anticipated that no special calibrations will be needed for these types of material. Clay minerals have widely varying electromagnetic properties that depend on the clay type and moisture level. Due to the wide variation of clay minerals, fouling that consists of these minerals may be difficult to estimate. It should be noted that to some scientists, "clay" is a very fine-grained material and has nothing to do with mineralogy. If these fine-grained clays are derived from granite, limestone, or coal, then the RABIT should not have difficulty in making reasonable moisture and fouling estimates.

Future plans include testing at various locations on BNSF revenue service track. This testing will involve RABIT measurements, ballast sample extraction, and laboratory measurements of moisture and fouling. During the course of this testing, ESS will examine a waveform picking algorithm, continue neural network training, and improve user software. For the foreseeable future, the focus will be on timber ties and fouling derived from granite, limestone, and coal. Testing with concrete ties has not yet been scheduled.

7. References

Al-Qadi, I., Wie, X., and Roberts, R. (2007, January). Scattering Analysis of Railroad Ballast Using Ground Penetrating Radar. Transportation Research Board Annual Meeting, Washington DC.

ASTM International (2007). Annual Book of Standards, Volume 04.08, Soil and Rock (1): D420 - D4914. ASTM International, Philadelphia, PA.

ASTM International (2008). Annual Book of Standards, Volume 04.08, Soil and Rock (II): D5714 – Latest. ASTM International, Philadelphia, PA.

Ayers, M., Thompson, M., and Uzarski, D., 1989, Rapid Shear Strength Evaluation of In Situ Granular Materials, Presented at Transportation Research Board 68th Annual Meeting, Jan. 1989, Washington D.C., Paper no. 880387.

Federal Railroad Administration (2014). Final Report for FRA-TR-010: Ballast Fouling Measurement Tool – Phase I. [DOT/FRA/ORD-18/33].Washington, DC: U.S. Department of Transportation.

Géron, A., 2017, Hands-On Machine Learning with Scikit-Learn and TensorFlow, O'Reilly Media, Inc., 1005 Gravenstein Highway North, Sebastopol, CA, 541 p.

Hagan, M. T., Demuth, H., B., Beale, M. H., Jesús, O., 2014, Neural Network Design, 2nd Edition, eBook, http://hagan.okstate.edu/NNDesign.pdf.Oden, C. P. (2006). *Calibration and Data Processing Techniques for Ground Penetrating Radar Systems with Applications in Dispersive Ground* (Doctoral dissertation). Colorado School of Mines, Golden, CO.

Powell, W.D., Potter, J.F., Mayhew, H.C., and Nunn, M.E. (1984). The Structural Design of Bituminous Roads [LR 1132]. Crowthorne, Berkshire, U.K.: Transport and Road Research Laboratory.

Rubin, A.J., Ho, C L., and Oden, C.P. (2018). A Comparison of Railroad Ballast Elastic Modulus as Estimated from Lightweight Deflectometer (LWD) and Dynamic Cone Penetrometer (DCP). Transportation Research Board Annual Meeting, Washington DC.

Selig, E. T., and Waters J. M. (1994). *Track Geotechnology and Substructure Management.* London: T. Telford.

Silvast, M., Nurmikolu, A., Wiljanen, B., and Levomaki, M. (2010). An Inspection of Railway Ballast Quality Using Ground Penetrating Radar in Finland. *Proceedings of the Institution of Mechanical Engineers, Part F: Journal of Rail and Rapid Transit, 224,* 345.

Webster, S.L., Grau, R.H. and Williams, R.P., 1992, Description and Application of Dual Mass Dynamic Cone Penetrometer, U.S. Army Engineer Waterways Experiment Station, Report No. GL-92-3.

Yoo, T.S., Chen, H.M., and Selig, E.T. (1978, March). Railroad Ballast Density Measurement. *Geotechnical Testing Journal, 1*(1), 41–54.

Abbreviations and Acronyms

ACRONYM	DEFINITION
ASTM	American Society for Testing and Materials
BNSF	Burlington Northern Santa Fe
CBR	California Bearing Ratio
DCP	Dynamic Cone Penetrometer
DPI	DCP Penetration Index
EM	Electromagnetic
ESS	Earth Science Systems, LLC
FEM	Finite Element Modeling
FRA	Federal Railroad Administration
GPR	Ground Penetrating Radar
LWD	Light-Weight Deflectometer
MLP	Multi-Layer Perceptron
RABIT	Radar Ballast Inspection Tool
UMass	University of Massachusetts